Received: 15 August 2021 | Revised: 23 September 2021 | Accepted: 29 September 2021

DOI: 10.1111/ijac.13931

International Journal of Applied Ceramic Technology

SPECIAL ISSUE ARTICLE

Short fiber-reinforced oxide fiber composites

Jonas Winkelbauer | **Georg Puchas** | **Stefan Schafföner** | **Walter Krenkel**

Department of Ceramic Materials Engineering, University of Bayreuth, Bayreuth, Germany

Correspondence
Jonas Winkelbauer, Department of Ceramic Materials Engineering, University of Bayreuth, Prof.-Rüdiger-Bormann-Str. 1, 95447 Bayreuth, Germany.
Email: jonas.winkelbauer@uni-bayreuth.de

Funding information
European Regional Development Fund, Grant/Award Number: 20-3066-03-18

Abstract

This paper presents a novel fiber spraying process for the manufacturing of short fiber bundle-reinforced Nextel™ 610/Al_2O_3-ZrO_2 oxide fiber composites (SF-OFC) and its characterization. First, the influence of varying fiber lengths (7, 14, and 28 mm, continuous fibers) and fiber orientations (unidirectional 0°, quasi-isotropic, ±45°) was investigated using hand-laid SF-OFC. Due to the weak matrix, the hand-laid material exhibited a strongly fiber-dominated material behavior, that is, variations in fiber length and orientation had a strong influence on the material properties. Second, the automated sprayed SF-OFC, however, exhibited a random orientation of the fiber bundles, which resulted in in-plane isotropic material properties. Average bending strengths of up to 177 MPa, strains of .39%, and a quasi-ductile fracture behavior were achieved. The strain was, therefore, in the range of fabric-reinforced OFC. While the bending strength of the SF-OFC was somewhat lower than that of fabric-reinforced OFC with the fiber orientation parallel to the loading direction, it was more than two times higher than the strength in 45° direction relative to the fabric reinforcement. Combined with good drapability and lower material costs compared to fabric-reinforced OFC, SF-OFC is, therefore, a promising material for industrial applications.

KEYWORDS
ceramic matrix composites, composites, fabrication, fibers, oxides

1 | INTRODUCTION

Oxide fiber composites (OFCs) have an exceptional lightweight construction potential and can be used in corrosive atmospheres at temperatures of up to 1100°C.[1] For such applications, high-performance oxide fibers, including Nextel™ 610 and Nextel™ 720, are used as reinforcing fibers.[1,2] These reinforcements are mainly used as continuous fibers, in the form of woven fabrics,[2–12] unidirectional (UD) layers,[13–15] or braiding.[4,16] However, only few studies[17–22] dealt with Nextel™ 610 short fiber-reinforced oxide ceramics.

Even for nonoxide ceramic matrix composites (CMCs), which have already achieved higher technology readiness levels than oxide CMC, there are only few tribological applications of short fiber-reinforced materials, for example, ceramic brake disc. In general, the use of short fiber reinforcements instead of continuous fiber reinforcements, such as fabrics, allows better drapability around narrow radii or spherical geometries, and thus, the

Honoring Dr. Mrityunjay Singh

realization of complex components by near-net shaping or forming. Furthermore, the use of short fibers instead of woven fabrics results in a material cost reduction of up to 30% for the same fiber volume content.[6] When using rovings with higher filament counts, material costs can be reduced up to 60%.[23,24] Increased automation could lower costs even further. Regardless of the reinforcing fiber and matrix, a random orientation of the fibers is usually desired for short fiber composites. In contrast to fabrics, there are no preferred directions in the plane. The composite, therefore, exhibits in-plane isotropic mechanical properties or only a slightly preferred fiber bundle direction.[24] Fabrics, on the other hand, exhibit a strong anisotropy. Thus, a previous study reported that the tensile strengths of an OFC with a fiber volume content of 48% decreased from 300 MPa, in 0°/90° direction, to about 60 MPa in ±45° direction.[2] Considering the bending strength, the strength decreased from 237 MPa (0°/90°) to 69 MPa in off-axis orientation (±45°).[24]

In addition to the lack of processing capabilities, there are currently no theoretical models to understand the fracture behavior of oxide short fiber bundle-reinforced oxide matrix composites (SF-OFCs) with quasi-ductile fracture behavior. For OFC in general, this quasi-ductility, which leads to damage tolerance and high thermal shock resistance, is usually realized by a porous matrix. Cracks are deflected or branched at the pores, and since there are only point contacts between the fibers and the matrix, cracks are also deflected along the fiber/matrix interface. This concept to achieve a damage tolerant fracture behavior of CMCs is known as the weak matrix concept (WMC).[25]

Short fiber-reinforced OFCs can be produced automatically via ceramic injection molding or a fiber spraying process. Currently, there are two[17–20] known research activities on ceramic injection molding of complex near-net-shape OFC components. Previous studies reported that during the injection molding process (kneading, extrusion, and injection), Nextel™ 610 fiber bundles were broken, separated into single fibers, and oriented. Tülümen et al.[18] described that the fiber length decreased from 3200 μm in the feedstock to only 200–300 μm in the sintered OFC. Both studies did not discuss the fracture behavior of the short fiber-reinforced OFC in detail, but Böttcher et al.[20] mentioned that a damage tolerant fracture behavior was not achieved.

In previous studies,[21,22] however, we developed and patented two processes for the production of damage-tolerant SF-OFC, using Nextel™ 610 short fiber bundles and a slurry. The first process involves the production of a short fiber bundle preform, which is stabilized by a liquid binder, and subsequently infiltrated with a slurry, which is then dried and finally sintered.[21] The second process is a fiber spraying process for SF-OFC, which was adapted from a common process for the production of glass and carbon fiber-reinforced plastics.[22] It was shown that in order to obtain a damage tolerant fracture behavior, the fiber bundle structure needs to be preserved. Additionally, the fiber bundles have to be completely infiltrated with a low viscosity slurry in order to mechanically decouple the single fibers from each other. This allowed the fabrication of SF-OFC with a fiber volume content of 21%, an apparent porosity of 40 vol%, and a mean bending strength of 90 MPa, independent of the loading direction.[24] While the basic feasibility of the process was demonstrated, there is currently no detailed investigation of the mechanisms of short fiber bundle-reinforcements, as they already partly exist for nonoxide short fiber CMCs.[24]

In a previous study together with the Chair for Robotics and Embedded Systems (University of Bayreuth), we designed and built an automated fiber spraying system,[26] which in the future could allow the reproducible production of SF-OFC. This work deals on the one hand with a basic investigation of hand-laid short fiber-reinforced OFC with regard to fiber orientation and length. On the other hand, the automated manufacturing of SF-OFC using the novel short fiber spraying process will be analyzed.

2 | EXPERIMENTAL PROCEDURE

This investigation involved the preparation of SF-OFC samples, which were either manufactured by hand lay-up or an automated fiber spraying process. Their microstructure and mechanical properties were subsequently characterized.

2.1 | Materials

In this study, sized Nextel™ 610 10 000 den high purity α-alumina fiber bundles (3 M Corporation, St. Paul, MN, USA) were used as reinforcing fibers. Polyvinyl alcohol sizing was necessary for processing the rovings and preserving the bundle structure of the short fibers. In previous investigations,[24] it was already demonstrated that despite the use of sized fibers for fiber spraying, the resulting damage tolerant fracture behavior is similar to that of desized long fiber-reinforced OFC. Two slurries with differing solid content were processed. A slurry with 67 wt% solid content was selected for manual infiltration of the fiber bundles, and a sprayable, low viscosity slurry with 60 wt% solid content was used for fiber spraying. The solid content of both slurries was composed of 25 wt% 3YSZ (TZ-3Y-E, Tosoh, Japan) and 5 wt% alumina powder (TM-DAR, Taimicron, Japan) sintering-active powders ($d_{50} \approx .1\ \mu$m) and 70 wt% larger ($d_{50} \approx 1\ \mu$m), sintering-sluggish alumina

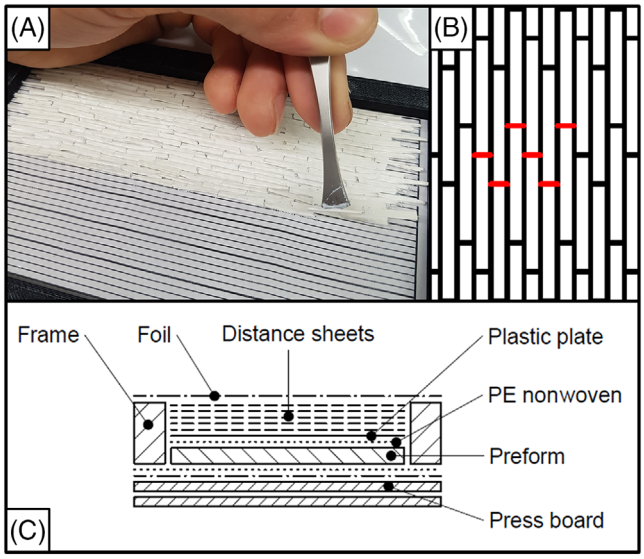

FIGURE 1 (A) Manual placement of the preimpregnated short fiber bundles, (B) placement pattern with offset joints, and (C) schematic press assembly

powder (CT-3000 SG, Almatis, OYAK, Turkey). Distilled water, 1.5 wt% Sokalan PA15 dispersant (BASF, Germany) and 26 wt% glycerol (99.5% AnalaR NORMAPUR®, VWR, Germany), in relation to the solid content, made up the liquid phase. The glycerol exhibits hygroscopic properties, which allowed the adjustment of the water content of the slurry and thus the required tack of the preimpregnated fiber products (prepregs) for lamination.[5,6,27] Based on the total mass of the slurry, .5 wt% binder (PLEXTOL™ B 500, Synthomer plc, UK) was added in order to facilitate vacuum bagging.

2.2 | Hand lay-up

In contrast to the samples from the previous studies[24] with fiber volume contents around 40 vol%, specimens with a fiber volume content of 26–29 vol% were prepared in this study. This was expected to improve comparability with sprayed short fiber-reinforced composites, due to their fiber volume content of around 28 vol%. To separately investigate the influence of the fiber length and fiber orientation, individual fiber bundles were infiltrated with the slurry and conditioned for 1 h at 50°C in a drying cabinet (FDL 115, Binder, Germany). Subsequently, the preinfiltrated fiber bundles exhibited the desired tack, allowing them to be cut to the required length (140, 28, 14, and 7 mm) using a punching tool. Then, they were deposited individually in the desired orientation–UD 0° $(45°/-45°/45°/-\overline{45}°)_S$ and quasi-isotropic $(0°/90°/45°/-45°)_S$. As shown in Figure 1A, the fiber bundles were individually applied

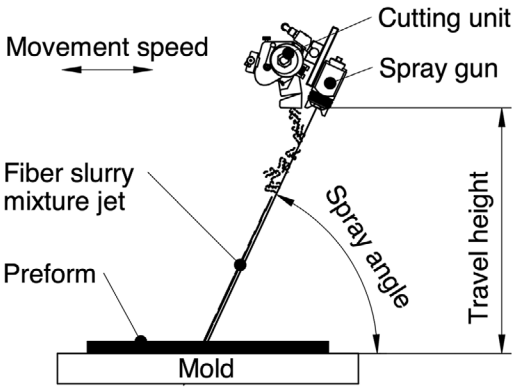

FIGURE 2 Schematic illustration of the fiber spraying process

to a width of 2 mm in the respective orientation of the layer, resulting in a grammage of 555 g/m^2. The individual short fiber bundles were laid up in an offset arrangement according to Figure 1B in order to prevent joints from overlapping in the in-plane and in the thickness direction. After one layer was laid up, eight individual layers or, in the case of the ± 45° specimens, seven layers with a symmetrical structure were laminated to obtain a specimen of 140 × 80 mm^2. The laminated sheets were conditioned in a climate chamber (305SB/+10 IU, Weiss, Germany) at 25°C and at a humidity of 53%. Subsequently, they were pressed with a cold roll laminator.

Due to the cold roll laminator and the use of a frame (Figure 1C), the individual bundles were prevented from slipping apart and the packing of the discrete fiber bundles was improved. Hence, macropores in the microstructure were prevented and disturbance variables were minimized. For this process, the preforms, covered on both sides with a polyethylene (PE) nonwoven, a plastic plate, and distance sheets, were placed in the frame as shown in Figure 1C. The distance sheets were inserted gradually, creating a successive compaction of the laminate. The final thickness of the laminates was about 3 mm. After the pressing process, the laminates were dried in the drying cabinet at 60°C for 2 h, followed by drying at 100°C for 12 h. Afterward, the green bodies were sintered in a furnace (LH 60/14, Nabertherm, Germany) at 1225°C for 2 h in air.

2.3 | Fiber spraying process

In the fiber spraying process, as shown in Figure 2, sized continuous fiber bundles were chopped by a cutting unit to bundles of 14 mm length, before being ejected into a slurry spray.[22] The slurry was supplied via a pressure feeding container to a high-volume, low-pressure automatic spray gun where it was atomized. The fiber bundles were infiltrated by the slurry in-flight and piled up on the mold

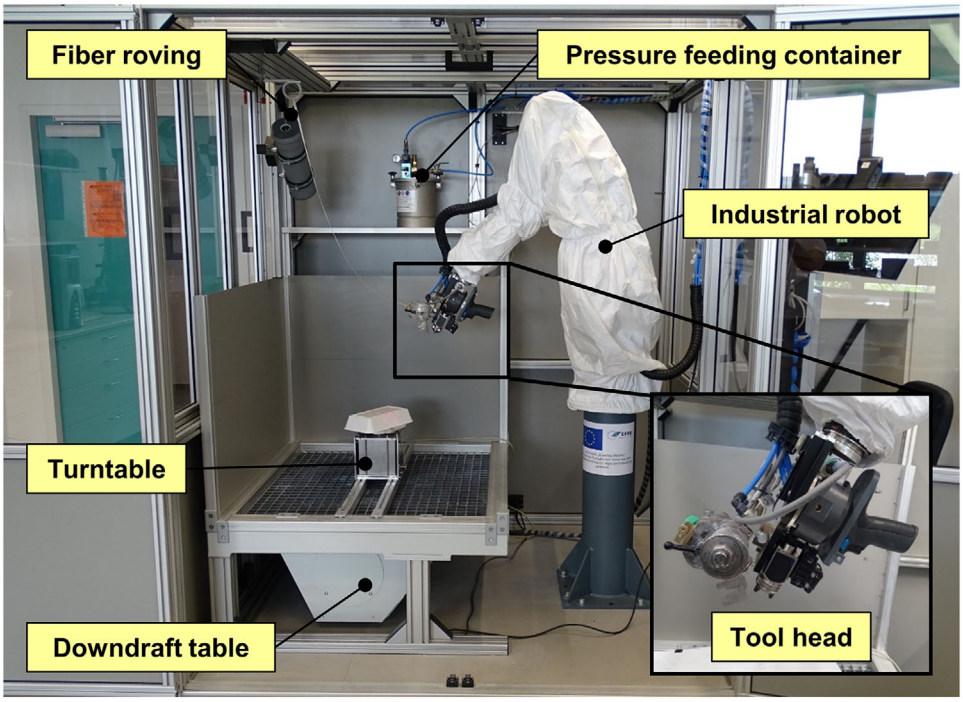

FIGURE 3 Automated fiber spraying system at CME

layer by layer, together with excess slurry.[22] To adjust the spray pattern, the slurry jet geometry was tailored to the process via pneumatic nozzles (round and flat jet). As shown in Figure 3, all described components were mounted at the end of a 6-axis industrial robot (TX2-90L, Stäubli International AG, Switzerland). The trajectory was programmed with a standard program on the teaching pendant of the robot. All components of the tool head were pneumatically controlled.

The fiber spraying process for OFC was originally developed using a linear slide, on which the fiber spraying unit (spray gun and cutting unit) was manually moved.[6,24] This experimental setup of 400 mm travel height, 65° spray angle, and .32 m/s travel speed (Figure 2) proofed to be advantageous in order to obtain SF-OFC with a quasi-ductile fracture behavior comparable to fabric-reinforced OFC. Therefore, this parameter set was also used for initial tests with the automated fiber spraying approach described by Schmidt et al.[26] These tests were performed by conventionally programming a linear track of 400 mm length. A dense spray pattern was achieved over a width of approximately 100 mm width. For each sample in this work, the linear track was run four times in order to build up a sufficient thickness. After the spraying process, the preimpregnated fibers (prepregs) were manually precompacted and vented using a finned roller, before being predried for 1 h at 50°C in a drying cabinet in order to activate the binder contained in the slurry. Subsequently, the tack of the prepregs was adjusted in a climate chamber at 25°C and a humidity of 53%. Two sprayed SF-OFC samples were prepared. For the first plate, the conditioned prepregs were cut into three 140×80 mm^2 pieces, which were then laminated together and pressed identically to the hand-laid laminates using a cold roll laminator and a frame with different densification inserts (Figure 1). After successive compaction, the laminate thickness was about 2.3 mm. The second plate was prepared without a lamination step. In this case, a 260×100 mm^2 sheet was cut from the conditioned prepreg, covered on both sides with a PE nonwoven, and pressed between two plates in a vacuum bag. Vacuum was first drawn at room temperature for 2 h, and then in a drying cabinet at 60°C for an additional 12 h. After removing the vacuum bag, the self-supporting green bodies were dried for 12 h at 100°C and sintered at 1225°C for 2 h in air.

2.4 | Characterization

The sintered OFCs were cut to a size of 80×250 mm^2 for the sprayed ones and 140×70 mm^2 for the hand-laid ones, using a water-cooled diamond wire saw (Type 6234, Well, Germany). The density and porosity were determined by Archimedes' principle.

To determine the fiber volume content of the sprayed samples, a 100×30 mm strip was taken in the green body condition, the fibers were then washed out in order to remove the green matrix, before they were dried and weighed. The fiber volume content of the strip was

TABLE 1 Mean bending strengths, strains, fiber volume contents, and porosities of unidirectional (0°) hand-laid fiber bundle-reinforced OFC and the monolithic Al_2O_3-ZrO_2 matrix

	Bending strength [MPa]	Strain [%]	Fiber volume content [vol%]	Porosity [%]
Matrix	54 ± 12	.16 ± .04	–	38.5
7 mm short fibers (0°)	67 ± 15	.15 ± .03	28.6	35.0
14 mm short fibers (0°)	100 ± 16	.20 ± .03	25.6	34.8
28 mm short fibers (0°)	158 ± 19	.22 ± 0.03	28.7	33.6
Continuous fibers (0°)	272 ± 28	.34 ± .06	26.9	31.3

calculated using the determined fiber mass and fiber density (3.9 g/cm^3)[28] and extrapolated to the volume of the OFC. For the hand-laid OFC, the amount of fibers per plate is known due to the manual production process. The volume of both OFC was calculated from the mass of the OFC before cutting and the density was determined by Archimedes' principle. The fiber volume content of the OFC was calculated from the fiber volume and the volume of the OFC. The water-cooled diamond wire saw was used for specimen preparation of the bending specimens. The hand-laid and the sprayed and laminated OFC were prepared in 0° direction (ten 70 × 10 mm^2 specimens each). For the sprayed and vacuum-pressed OFC, five test specimens each (50 × 10 mm) were prepared in 0°, 45°, and 90° orientations, with respect to the spraying direction. A three-point bending test was performed on a universal testing machine (inspekt 5 table blue, Hegewald & Peschke, Germany) according to DIN 658-3.[29] A fixed support span of 60 mm was selected for the hand-laid specimens. The component thickness of the sprayed and vacuum-pressed plate was .71 mm. To comply with the standard length/thickness ratio of 20,[29] the support span was adjusted to 15 mm.

A scanning electron microscope (SEM) test specimen was taken from each OFC using the water-cooled diamond wire saw, which was then embedded in epoxy resin, ground, and polished. The epoxy resin was subsequently burned out at 700°C, and the samples were sputtered with gold for 2 min at a pressure of .1 mbar and a current of 30 mA. The analysis of the microstructure was performed using an SEM (Zeiss Sigma 300 VB, Zeiss, Germany).

It was impossible to readily determine the fiber orientation in the sintered OFC. To provide an impression of the fiber orientation, a single layer was sprayed onto a transparent plastic film using the same process parameters of the sprayed specimens. This single layer was dried at room temperature and a field of 70 × 110 mm^2 was photographed at three positions on a transmitted light table. The evaluation of the images was carried out by the OrientationJ plugin of the open-source software ImageJ. The resulting histogram showed the fraction of fibers in each direction in the range from −90° to +90°.

3 | RESULTS AND DISCUSSION

3.1 | Fiber length

For a better understanding of SF-OFC, the mechanical properties as a function of the fiber length were investigated on hand-laid specimens. In Table 1, the bending strengths of the hand-laid UD specimens, together with the corresponding strain, fiber volume contents, and porosities, are given. For an evaluation of the fracture behavior, the stress-strain curves of representative specimens are shown in Figure 4. In addition to the OFC, the curve of the unreinforced monolithic matrix is also shown. It exhibited brittle fracture behavior with a mean bending strength of 54 ± 12 MPa. A damage-tolerant fracture behavior was already realized by a short fiber bundle of 7 mm, although no significant increase in strength (67 ± 15 MPa) was evident. The bending strength of OFC rose with increasing fiber length. A maximum mean bending strength of 272 MPa was obtained for continuous fiber-reinforced specimens. Bending strains also increased with increasing fiber length from .15% (7 mm short fibers) to .34% for the specimens with continuous fibers. A propagating crack can be deflected along an increasingly longer fiber. This resulting crack deflection leads to increased energy dissipation and finally to an enhanced strain and the required damage-tolerant fracture behavior.

Currently, there are no models for determining the critical fiber length of OFC, that is, the minimal fiber length leading to a reinforcing effect of the weak matrix. Only calculation models for the critical fiber length from fiber-reinforced plastics are currently known. Both fiber-reinforced plastics and OFC with a weak matrix exhibit a strongly fiber-dominated behavior. As a first approximation, the critical fiber length was, therefore, calculated according to Ehrenstein and Wurmb.[30] The calculation was based on the fiber strength (2800 MPa),[28] fiber diameter (12 μm),[28] and the interface shear strength reported in the literature for a porous OFC with Nextel™ 720 fibers and a matrix consisting of 80 wt% mullite and 20 wt% alumina (4.8 MPa).[31] According to this calculation, the

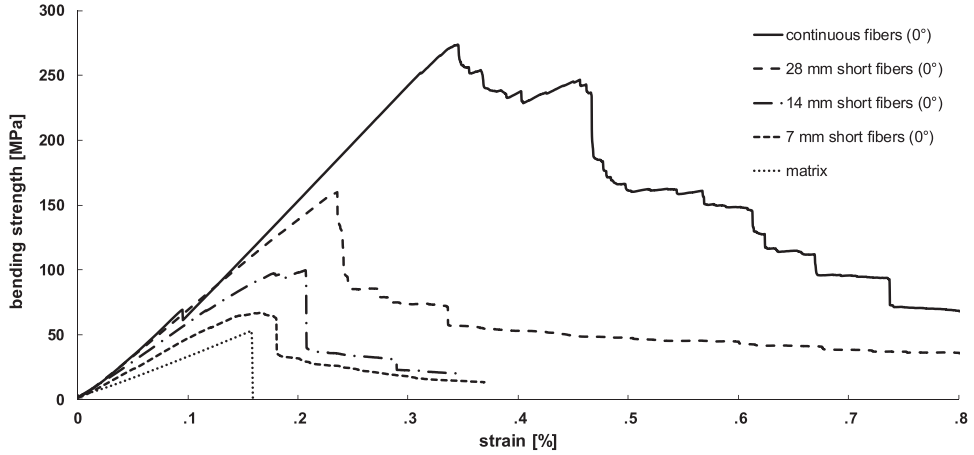

FIGURE 4 Representative stress-strain curves of unidirectional (0°) hand-laid fiber bundle-reinforced OFC and the monolithic Al_2O_3-ZrO_2 matrix

TABLE 2 Mean bending strengths, strains, fiber volume contents, porosities, and bending strengths normalized to a fiber volume content of 25 vol% of hand-laid fiber bundle-reinforced OFC with different fiber lengths and orientations

	Bending strength [MPa]	Strain [%]	Fiber volumecontent [vol%]	Porosity [%]	Normalizedbending strength [MPa]
Continuous fibers (0°)	272 ± 28	.34 ± .06	26.9	31	253 ± 26
14 mm short fibers (0°)	100 ± 16	.20 ± .03	25.6	35	98 ± 16
Continuous fibers (quasiisotropic)	180 ± 20	.31 ± .03	26.8	35	168 ± 19
14 mm short fibers (quasi-isotropic)	116 ± 16	.17 ± .01	29.0	32	100 ± 14
Continuous fibers (±45°)	61 ± 7	.30 ± .04	27.1	35	57 ± 7
14 mm short fibers (±45°)	61 ± 10	.23 ± .05	26.9	32	57 ± 9
Sprayed 14 mm short fibers (randomly oriented)	177 ± 16	.39 ± .04	28.0	39	158 ± 14

critical fiber length is 3.5 mm. All fiber lengths considered in this study were above this critical fiber length, resulting in a reinforcement effect and the presence of a quasi-ductile fracture behavior.

3.2 | Fiber orientation

For an evaluation of the influence of fiber orientation, the average bending strengths (average and normalized), strains, as well as the fiber volume contents and porosities are listed in Table 2. Corresponding to the continuous specimens with ±45° lay-up, the strength of the short fiber-reinforced specimens with ±45° orientation was also 61 MPa, that is, in the range of the matrix strength (Table 1). This is not surprising, because due to their brittle matrix, WMC exhibits a strongly fiber-dominated fracture behavior. Since there were no fibers oriented parallel to the loading direction, the bending strength could not exceed the matrix strength. Nevertheless, the fibers allowed the deflection of cracks, resulting in damage-tolerant fracture behavior.

Unsurprisingly, the highest bending strengths (272 ± 28 MPa) were achieved with continuous fiber-reinforced UD specimens. This is due to the fact that all fibers are orientated in the loading direction, whereas the amount of fibers in loading direction was lower for the quasi-isotropic (180 MPa) and ±45° (61 MPa) specimens. A different correlation between fiber orientation and resulting bending strength was found for the SF-OFC. Considering the normalized bending strengths (Figure 5), only small differences can be identified between the 14 mm quasi-isotropic (100 MPa) and 14 mm UD (98 MPa) reinforced, hand-laid specimens. The strength of the laminate appears to be determined only by the two outer layers, which were loaded in tension and compression during the bending test. These were oriented in the loading direction (0°) for the UD specimens as well as

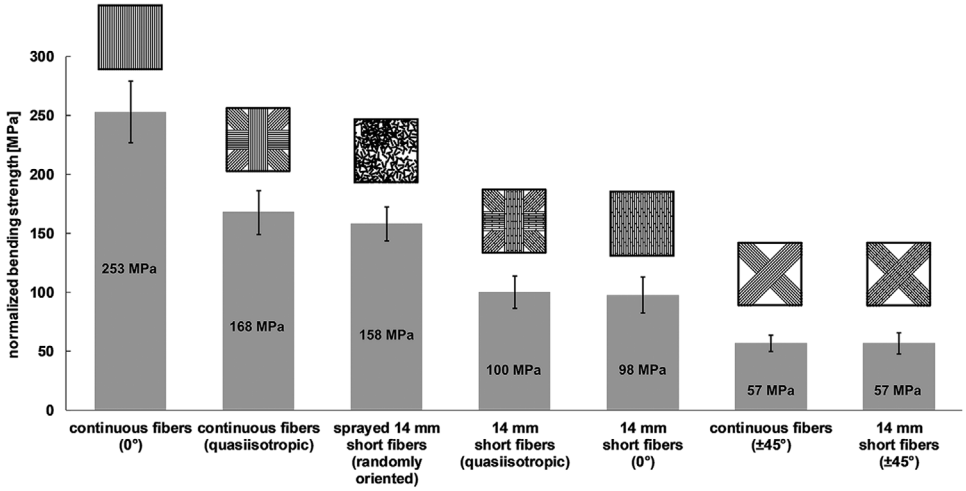

FIGURE 5 Comparison of bending strengths of hand-laid fiber bundle-reinforced OFC with different fiber length and orientation (normalized to a fiber volume content of 25 vol%)

for the quasi-isotropic specimens. However, short fibers can absorb significantly lower tensile forces than long fibers, which on the one hand reduces the strength of the OFC (Figure 4), and on the other hand decreases the influence of fiber orientation. Nevertheless, regardless of fiber orientation, crack deflection and branching can be achieved by short fiber reinforcements. In the three-point bending test, the tensile stress can be absorbed to a certain degree by the short fibers, and any crack that occurs can first be deflected along the short fibers oriented in the loading direction on the tensile side. As soon as the crack reaches a joint between two fibers, it will propagate unhindered through this matrix area and the entire first layer will fail. The crack will subsequently break through the weak points in the composite (joints), regardless of the orientation of the short fibers, until the whole composite fails. Therefore, no difference was finally detected between UD and quasi-isotropic laminates with short fiber reinforcement. For the quasi-isotropic specimens with continuous fibers, only the two outer layers were oriented parallel to the loading direction as well. However, the fiber orientation of the middle layers of the composite had a much stronger effect in this case, leading to a far more pronounced difference between the UD and quasi-isotropic laminate structure. As soon as a single fiber fails on the tensile side, the tensile stress can be transferred to an adjacent fiber, which is also oriented in the direction of the load, until it also breaks.[32] This continues until the entire layer oriented in the load direction fails. In a UD laminate, this mechanism is possible over the entire specimen thickness, which means that higher strengths can be achieved compared to quasi-isotropic laminates, where the outer 0° layers are followed by a 90° layer, which cannot absorb the load.

In Figure 5, it can be seen that these continuous fiber-reinforced specimens with quasi-isotropic structure (168 MPa) were at the same strength level as the sprayed randomly oriented 14 mm SF-OFC (158 MPa). In the sprayed specimens, fibers were distributed randomly over the entire specimen thickness. Based on this fact, it has to be investigated whether the use of sandwich structures with continuous fiber-reinforcement in the outer layers and cost-efficient randomly oriented short fibers in the core is effective or if a pure short fiber-reinforcement provides sufficient strength. A detailed analysis of this question should be considered in future studies.

Analyzing the average strains in Table 2, it can be seen that the specimens with continuous fiber reinforcements, regardless of orientation, achieved a strain of about .30%. By contrast, strains of approximately .20% were observed for the hand-laid short fiber-reinforced specimens due to the fact that the crack deflection length of the continuous fibers was higher than for short fibers. Only the sprayed short fiber specimens with random fiber orientation achieved strains averaging .39%, which was above the strains of continuous fiber-reinforced specimens. The microstructure revealed that the sprayed OFC exhibited a slightly spliced bundle structure (Figure 6A). By contrast, quasi-isotropic specimens with continuous fibers had strongly isolated fibers in the respective layers (Figure 6B). This isolation of the fibers was observed in all hand-laid samples. Isolated fibers are generally less resistant to cracks, and transfer of stress between the fibers is more difficult due to the large distance between them, which leads to decreased bending strength. Levi et al.[32] described that a CMC with a weak matrix should, in principle, be designed in a way that fiber fractures initially occur randomly after the formation of matrix cracks. The failure

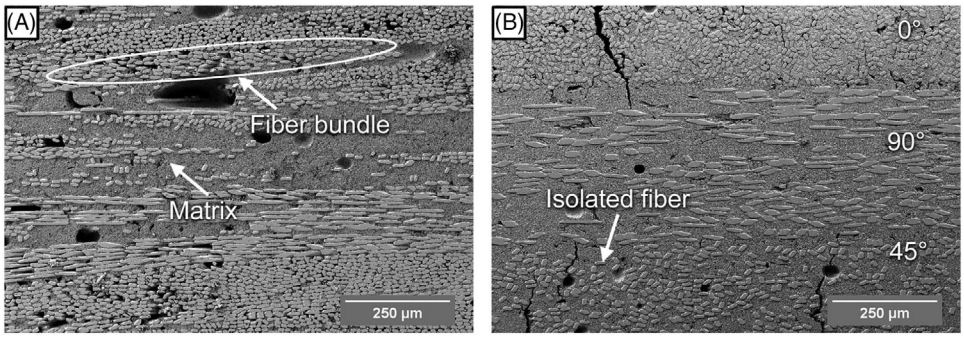

FIGURE 6 SEM images of the microstructure of (A) sprayed 14 mm short fibers (randomly oriented) and (B) hand-laid quasi-isotropic continuous fiber-reinforced OFC

TABLE 3 Mean bending strengths, strains, fiber volume contents, and porosities of sprayed fiber bundle-reinforced OFC pressed by cold roll laminator and vacuum bagging

Sprayed 14 mm short fibers	Bending strength [MPa]	Strain [%]	Fiber volume content [vol%]	Porosity [%]
Cold roll laminator	177 ± 16	.39 ± .04	28.0	39
Vacuum bagging	133 ± 27	.56 ± .10	28.2	40

of several fibers within a bundle then leads to a fiber bundle failure. Finally, several fiber bundle cracks connect through the intervening matrix regions causing the final failure of the composite. However, since this bundle structure was missing in the hand-laid OFC, the crack initiation was not sufficiently delayed and the crack could propagate unhindered through the matrix areas. It appears that the random orientation as well as the preservation of the slightly spliced bundle structure allowed more deflection and branching of cracks. These increasing energy dissipations were reflected by increased strains. The transfer of stress between the fibers was possible due to the small distance between them, which leads to increased strength values, although effectively less fibers were oriented in the direction of the load than in the 14 mm short fibers (0°) sample. For short fiber-reinforced OFC, the influence of the bundle structure seems to be more significant than the orientation of the fibers in the loading direction.

3.3 | Fiber spraying

For the implementation of complex geometries, the compaction of the laminates using a cold roll laminator is not feasible. Instead, the compaction of nonplanar components was realized via a press with a closed mold or vacuum bagging. In this first investigation of automatically manufactured SF-OFC, specimens pressed with a cold roll laminator were compared with vacuum-pressed specimens. The corresponding bending strengths and strains are given in Table 3 together with the fiber volume content and the porosity. The mean bending strength of the sample "sprayed 14 mm short fiber bundle-reinforced OFC (vacuum bagging)" is the average of all three test orientations 0°, 45°, and 90°. Representative stress-strain curves are shown in Figure 7. With both pressing processes, comparable fiber volume contents (28 vol%) and porosities (approximately 40%) were realized.

Figure 7 shows that both specimens exhibited damage-tolerant fracture behavior due to their fiber reinforcement. The average bending strength of the cold roll-laminated specimens was 177 MPa, and therefore about 25% higher than the 133 MPa of the vacuum-bagged OFC. These differences can be explained by different degrees of compaction due to the pressing processes. The flexing motion of the cold roll laminator made it possible to compact the prepregs more effectively. Using vacuum bagging, the prepregs were pressed statically, without any flexing motion, which allowed compaction only to a lower degree. Although the differences in fiber volume content and porosity were not apparent, the slightly higher porosity and fiber volume content of the vacuum-bagged sample indicated a lower macroporosity of the cold roll-laminated sample. Since the air bubbles in the matrix are normally less than 50 μm and in the fiber bundles less than 10 μm, more likely less than 5 μm, their removal or at least their decrease did not result in a significant change of the overall porosity. Far more importantly, the flexing motion of the cold roll lamination led to a more homogeneous microstructure, especially since it aided the infiltration of the fiber bundles. A homogeneously infiltrated fiber bundle is paramount for the WMC, because it enables

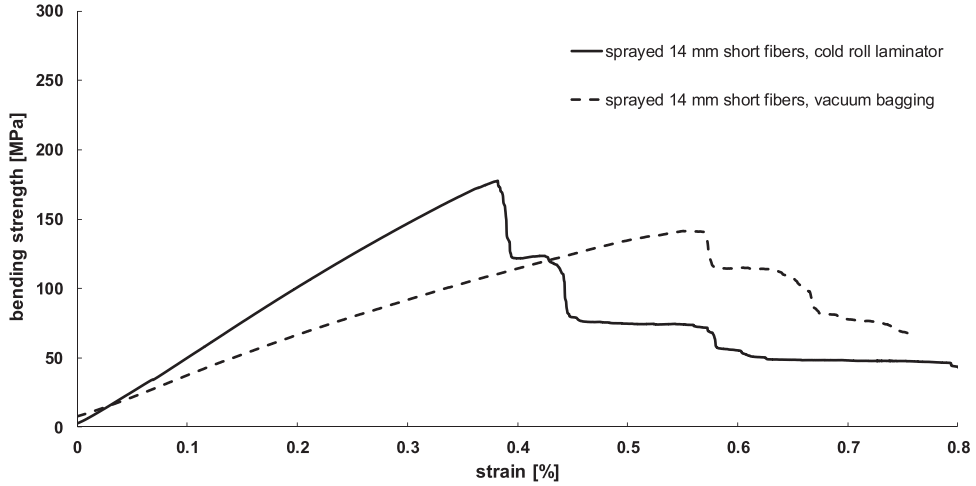

FIGURE 7 Representative stress-strain curves of a sprayed 14 mm short fiber bundle-reinforced OFC pressed by cold roll laminator and vacuum bagging

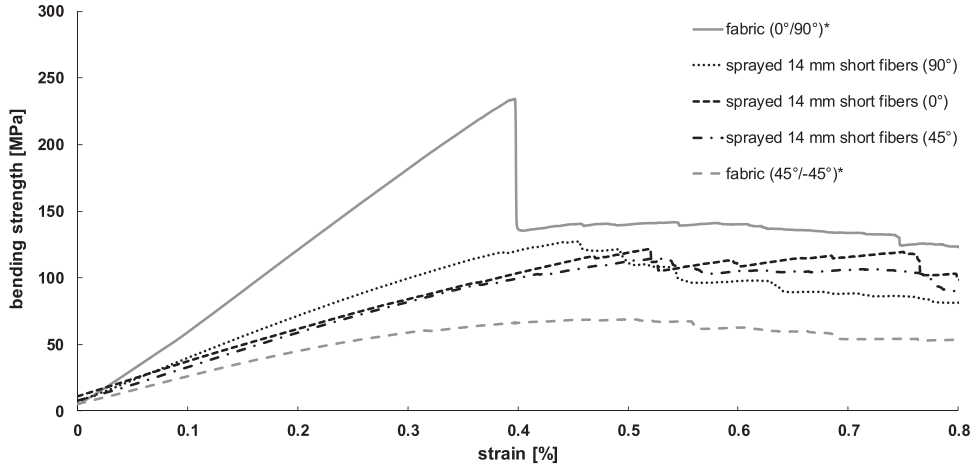

FIGURE 8 Representative stress-strain curves of fabric-reinforced (3000 den) specimens in the 0°/90° and ±45° directions, *described in previous studies[6] and sprayed 14 mm short fiber bundle-reinforced (10 000 den) OFC, divided into the three test directions 0°, 45°, and 90°, relative to the spray direction

the mechanical decoupling of the single filaments. It also explains the lower standard deviation of the cold roll-laminated specimens (177 ± 16 MPa) compared to the vacuum bagging ones (133 ± 27 MPa). In addition to the more homogeneous microstructure, the flexing motion of the cold roll laminator caused a slight movement of the fiber bundles during the lamination process. This allowed for a slight sliding of the bundles into each other, that is, interlocking of the bundles, which ultimately supported the crack deflection. In case of planar components, compaction by a cold roll laminator is, therefore, the most effective method. However, as mentioned above, this is not possible for the subsequent implementation of more complex component geometries, so that vacuum bagging or a press with a closed mold must be used for this purpose, albeit with a certain decrease in strength.

Figure 8 shows the bending strength of a fabric-reinforced OFC, based on preliminary investigations,[6] tested in the main direction (0°/90) and off-axis (±45°) together with representative curves (in terms of stress level and strain) of the "sprayed 14 mm short fibers (vacuum bagging)" specimen from Table 3 separated into the three test directions (0°, 45°, and 90°). At a comparable fiber volume content of 28 vol%, the bending strength of fabric-reinforced specimens was 237 MPa in the main direction (0°/90).[6,24] Considering the fact that only 50% of the fibers in a fabric are oriented in load direction, the strength appears high compared to the UD specimens with continuous fiber reinforcement (272 ± 28 MPa) presented in Table 1 and Figure 4. However, as mentioned before, the isolation of the fibers in the hand-laid OFC (Figure 6B) also plays a crucial role here. Due to isolated fibers, on

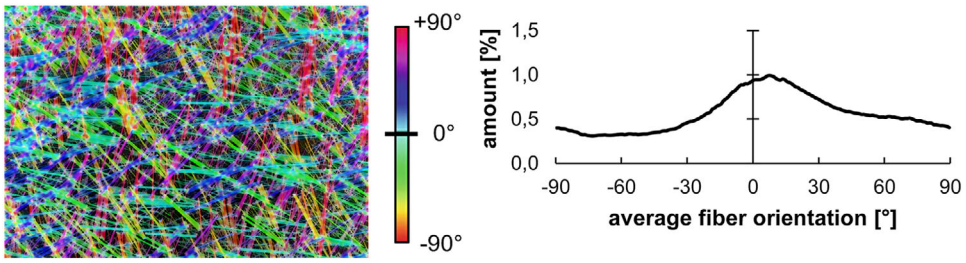

FIGURE 9 A representative single layer analyzed via ImageJ together with the average distribution curve of the fiber orientation of this sprayed 14 mm short fiber layer

the one hand, a crack that develops cannot be sufficiently branched or redirected, and on the other hand, the stress transfer between individual fibers is difficult to impossible if the distance between them is too large. These problems do not occur with woven fabrics, since here the bundle structure has been maintained by the textile structure with binding points. As a result, relatively high strengths could be achieved even though there were quantitatively less fibers in loading direction. The off-axis properties, however, decreased dramatically to 30% of the strength (69 MPa).[6,24] As already noted for the specimens with ±45° fiber orientation, no fibers were orientated parallel to the load direction. The strength was, therefore, determined solely by the matrix. Through the use of the fiber spraying process, it was possible to produce a material with comparable strains and a mean bending strength of 128 ± 16 MPa (0°), 126 ± 34 MPa (45°), and 144 ± 31 MPa (90°), respectively. The strength of the SF-OFC was, therefore, lower than that of the fabric-reinforced OFC in the main direction, but almost twice as high as the off-axis strength of the same fabric-reinforced OFC. Considering the standard deviation, the respective strengths of the SF-OFC were quite similar, that is, independent of the test direction. Consequently, the material can be seen as in-plane isotropic. This in-plane isotropy is a result of the random orientation of the fibers, which occurred automatically due to the process. The fiber bundles underwent a change in direction after being dragged by the slurry jet. Thereby, they were carried along, spread out, and thus randomly distributed over the width of the jet.

The fiber orientation of a single sprayed layer was analyzed via ImageJ. Example images of the single layers and the average distribution curve of the occurring fiber orientations are shown in Figure 9. From the images of the single layer, it can be deduced that in-plane, the fibers were randomly distributed. For the sprayed 14 mm short fiber specimen, a slightly preferred direction in 0° was detected. However, this proportion was in the range of only .5%. According to the strengths in Figure 8, this preferred direction could not be verified and is, therefore, negligible. The high strength deviation within a specimen is due to inhomogeneous material distribution. Particularly, in case of such thin samples (approx. .7 mm for the vacuum-bagged sample) as prepared in this study, the large variation needs to be critically assessed. In the loaded volume, for example, the fiber volume content as well as the orientation could vary locally leading to different amounts of fibers oriented favorably for load bearing. With thicker short fiber specimens, the probability of reinforcing fibers being present in the load direction increases. A detailed investigation of the component thickness and its influence on the variation of the strength should be considered in future investigations.

4 | CONCLUSIONS

The properties of short fiber bundle-reinforced OFCs, with regard to fiber length and orientation, were investigated for the first time in a fundamental study with hand-laid specimens. Due to the fiber-dominated material behavior, deviations of the fiber orientation from the test direction had a strength-reducing effect. A damage-tolerant fracture behavior was already achieved with 7 mm fiber length. Longer reinforcing fibers led to a strength increase. Unidirectionally oriented 14 mm short fibers achieved bending strengths of 100 MPa, 28 mm short fibers already 158 MPa, and continuous fiber bundles on average 272 MPa.

In addition, initial tests were carried out with the new automated fiber spraying system. The novel short fiber bundle-reinforced OFC material was then investigated. Sprayed prepregs can be directly pressed or processed via a laminating and forming step. Depending on the complexity, compaction can be performed by a cold roll laminator (planar geometries) or by pressing with a closed mold or vacuum bagging. The fiber spraying process enabled the manufacturing of an in-plane isotropic composite material with a bending strength of up to 177 MPa (pressed by cold roll laminator) and strains comparable to continuous fiber-reinforced OFC (approx. .4%). Like conventional fabric-reinforced OFC, they exhibited quasi-ductile fracture behavior, albeit at a lower strength level. Off-axis, however, the bending strength

of short fiber bundle-reinforced OFC exceeded the fabrics by more than double. This makes short fiber bundle-reinforced OFC a cost-efficient alternative for low-stress composites. Their good drapability also allows the fabrication of complex near-net-shape structures at a cost reduction of up to 60% (10 000 den fiber bundles) compared to the common DF-19 (3000 den fabric) reinforced composites.[23,24]

ACKNOWLEDGMENTS

The authors acknowledge Prof. Dr. Dominik Henrich and Edgar Schmidt from the Chair for Robotics and Embedded Systems (University of Bayreuth) for the excellent cooperation.

This work has partly been supported by the European Regional Development Fund (ERDF) under the project "Roadmap zur flexiblen Produktion individueller Produkte" (Roadmap flexPro) (EFRE 20-3066-03-18).

Open Access funding enabled and organized by Projekt DEAL.

REFERENCES

1. Wilson D, Visser L. High performance oxide fibers for metal and ceramic composites. Compos Part A. 2001;32(8):1143–53.
2. Simon RA, Danzer R. Oxide fiber composites with promising properties for high-temperature structural applications. Adv Eng Mater. 2006;8(11):1129–34.
3. Guglielmi PO, Blaese D, Hablitzel MP, Nunes GF, Lauth VR, Hotza D, et al. Microstructure and flexural properties of multilayered fiber-reinforced oxide composites fabricated by a novel lamination route. Ceram Int. 2015;41(6):7836–46.
4. Puchas G, Held A, Krenkel W. Near-net shape manufacture process for oxide fiber composites (OFC). Mater Today: Proc. 2019;16:49–58.
5. Puchas G, Möckel S, Krenkel W. Novel prepreg manufacturing process for oxide fiber composites. J Eur Ceram Soc. 2020;40(15):5930–41.
6. Puchas G, Krenkel W. Neuartige Herstellungsverfahren für oxidkeramische Faserverbundwerkstoffe (Novel manufacturing processes for oxide ceramic fiber composites). In: dIALOG Materialwissenschaft und Werkstofftechnik., 1 2018. 34–41.
7. Guglielmi PO, Nunes GF, Hablitzel M, Hotza D, Janssen R. Production of oxide ceramic matrix composites by a prepreg technique. MSF. 2012;727–728:556–61.
8. Ben Ramdane C, Julian-Jankowiak A, Valle R, Renollet Y, Parlier M, Martin E, et al. Microstructure and mechanical behaviour of a Nextel™610/alumina weak matrix composite subjected to tensile and compressive loadings. J Eur Ceram Soc. 2017;37(8):2919–32.
9. Almeida RSM, Pereira TFS, Tushtev K, Rezwan K. Obtaining complex-shaped oxide ceramic composites via ionotropic gelation. J Am Ceram Soc. 2019;102(1):53–7.
10. Wamser T, Scheler S, Martin B, Krenkel W. Novel oxide fiber composites by freeze casting. J Eur Ceram Soc. 2014;34(15):3827–33.
11. Levi CG, Yang JY, Dalgleish BJ, Zok FW, Evans AG. Processing and performance of an all-oxide ceramic composite. J Am Ceram Soc. 1998;81(8):2077–86.
12. Radsick T, Saruhan B, Schneider H. Damage tolerant oxide/oxide fiber laminate composites. J Eur Ceram Soc. 2000;20(5):545–50.
13. Cinibulk MK, Keller KA, Mah T-I. Effect of yttrium aluminum garnet additions on alumina-fiber-reinforced porous-alumina-matrix composites. J Am Ceram Soc. 2004;87(5):881–7.
14. Goushegir SM, Guglielmi PO, Da Silva JGP, Hablitzel MP, Hotza D, Al-Qureshi HA, et al. Fiber-matrix compatibility in an all-oxide ceramic composite with RBAO matrix. J Am Ceram Soc. 2012;95(1):159–64.
15. Schmücker M, Mechnich P. Microstructural coarsening of Nextel ™ 610 fibers embedded in alumina-based matrices. J Am Ceram Soc. 2008;91(4):1306–8.
16. Wilhelmi C, Machry T, Knoche R, Koch D. Processing of oxide/oxide composites for gas turbine applications based on braiding technique (OXITEX™). In: Singh D, Salem J, Widjaja S, editors. Mechanical properties and performance of engineering ceramics and composites VI. Hoboken, NJ: John Wiley & Sons, Inc; 2011. pp. 23–36.
17. Tülümen M, Hanemann T, Hoffmann MJ, Oberacker R, Piotter V. Process development for the ceramic injection molding of oxide chopped fiber reinforced aluminum oxide. KEM. 2017;742:231–7.
18. Tülümen HM, Hanemann T, Piotter V, Stenzel D. Investigation of feedstock preparation for injection molding of oxide–oxide ceramic composites. JMMP. 2019;3(1):9.
19. Piotter V, Tueluemen M, Hanemann T, Hoffmann MJ, Ehreiser B. Powder injection molding of oxide ceramic CMC. KEM. 2019;809:148–52.
20. Böttcher M, Nestler D, Stiller J, Kroll L. Injection moulding of oxide ceramic matrix composites: comparing two feedstocks. KEM. 2019;809:140–7.
21. Wamser T, Scheler S, Krenkel W. Method for the production of an oxide ceramic composite material and fiber preform. European Patent 2 848 599 B1. 2019.
22. Knohl S, Krenkel W, Martin B, Wamser T. Method for the preparation of an intermediate product for the manufacture of a fibre-reinforced part and device for carrying out same. European Patent 3 450 128 A1. 2021.
23. Lincoln J, Jackson B, Barnes A, Beaber A, Visser L. Oxide–oxide ceramic matrix composites—enabling widespread industry adoption. In: Mrityunjay S, Tatsuki O, Shaoming D, Dietmar K, Kiyoshi S, Bernd C, Bernhard H, Jun A, editors. Advances in high temperature ceramic matrix composites and materials for sustainable development, Ceramic Transactions. 263 2017;401–412.
24. Krenkel W, Flauder S, Puchas G. Short fiber ceramic matrix composites (SF-CMCs). In: Michael P, editor. Encyclopedia of materials: technical ceramics and glasses. 2 Amsterdam: Elsevier; 2021. pp. 260–76.
25. Zok FW. Developments in oxide fiber composites. J Am Ceram Soc. 2006;89(11):3309–24.
26. Schmidt E, Winkelbauer J, Puchas G, Henrich D, Krenkel W. Robot-based fiber spray process for small batch production. In: Schüppstuhl T, Tracht K, Henrich D, editors. Annals of

Scientific Society for Assembly, Handling and Industrial Robotics. Berlin, Heidelberg: Springer Berlin Heidelberg; 2020. pp. 295–305.
27. Knohl S, Krenkel W, Puchas G, Wamser T. Ceramic composite materials and method for producing same. International patent application WO 2017220727A9. 2017.
28. 3M™ Nextel™ ceramic fibers and textiles: technical reference guide. St. Paul, MN: 3M Advanced Materials Division; 2018.
29. DIN EN 658-3:2002-11, Hochleistungskeramik_- Mechanische Eigenschaften von keramischen Verbundwerkstoffen bei Raumtemperatur_- Teil_3: Bestimmung der Biegefestigkeit; Deutsche Fassung EN_658-3:2002: (Advanced technical ceramics — mechanical properties of ceramic composites at room temperature — Part 3: Determination of flexural strength; German version EN 658-3:2002).2002; Berlin: Beuth Verlag GmbH.
30. Ehrenstein GW, Wurmb R. Verstärkte Thermoplaste – Theorie und Praxis (Reinforced thermoplastics — theory and practice). Angew Makromol Chem. 1977;60(1):157–214.
31. Weaver JH, Rannou J, Mattoni MA, Zok FW. Interface properties in a porous-matrix oxide composite. J Am Ceram Soc. 2006;89(9):2869–73.
32. Levi CG, Zok FW, Yang JY, Mattoni M, Löfvander JPA. Microstructural design of stable porous matrices for all-oxide ceramic composites. Z Metallkd. 1999;90(12):1037–47.

How to cite this article: Winkelbauer J, Puchas G, Schafföner S, Krenkel W. Short fiber-reinforced oxide fiber composites. Int J Appl Ceram Technol. 2022;19:1136–1147. https://doi.org/10.1111/ijac.13931